J. Fluid Mech. (1971), *vol.* 47, *part* 1, *pp.* 113–125
Printed in Great Britain

Thermal convection with large viscosity variations

By K. E. TORRANCE AND D. L. TURCOTTE
Cornell University, Ithaca, New York

(Received 2 March 1970)

The influence of large variations of viscosity on convection in a layer of fluid heated from below has been investigated. Solutions for the flow and temperature fields were obtained numerically assuming infinite Prandtl number, free-surface boundary conditions, and two-dimensional motion of fixed horizontal wavelength. The effects of a temperature-dependent and a depth-dependent viscosity were each studied; calculations were also carried out using a temperature- and depth-dependent viscosity model appropriate to the earth's mantle.

1. Introduction

This paper presents a systematic numerical study of finite-amplitude convection in a fluid layer heated from below when the viscosity is a *strong* function of temperature and/or depth. Such flows are of interest in geophysics as well as in many technical processes.

Numerous investigators have studied thermal convection in a fluid with constant properties using analytic methods (Kuo 1961; Veronis 1966) or numerical calculations (Fromm 1965). Numerical solutions for thermal convection in a cylindrical container using a viscosity which varied linearly with temperature were obtained by Liang, Vidal & Acrivos (1969); however, the viscosity variation was insufficient to have a significant effect on flow patterns. Foster (1969*a*) has studied finite-amplitude convection in an internally heated fluid with a viscosity which increased exponentially with depth.

Thermal convection in a fluid with a viscosity which is a strong function of temperature and depth may be directly applicable to the earth's mantle. A comprehensive theory for continental drift has evolved in the past few years (McKenzie & Parker 1967; Morgan 1968; Le Pichon 1968; Isacks, Oliver & Sykes 1968). This theory pictures the crust of the earth as a series of plates, each plate being a segment of a sphere. These surface plates are created at oceanic ridges and are destroyed at oceanic trenches. Interactions between adjacent plates result in seismic activity, volcanism, and mountain building. The probable driving mechanism for the movement of the plates is thermal convection in the upper mantle (Oxburgh & Turcotte 1968; Elder 1968; McKenzie 1969). Ascending convection occurs beneath ridges and descending convection at oceanic trenches. Gordon (1965) has proposed that the fluid behaviour of the mantle can be explained by diffusion creep. This type of creep results in a Newtonian viscosity which is an exponential function of temperature and pressure (Herring 1950).

2. Formulation of the problem

Consider the convective flow of a viscous, heat-conducting fluid confined between two horizontal boundaries at distance h apart when a body force g acts downwards and the lower boundary is maintained at a higher temperature than the upper boundary, $T_h > T_0$. The flow is assumed to be laminar and two-dimensional. We take the thermal diffusivity κ and the coefficient of thermal expansion α to be constant; however, the viscosity may be a function of the temperature T and the vertical co-ordinate y.

Using primes to denote dimensional variables, we introduce the following non-dimensional quantities:

$$x = x'/h, \quad y = y'/h, \quad u = hu'/\kappa, \quad v = hv'/\kappa, \quad T = (T' - T_0')/(T_h' - T_0').$$

It is also convenient to introduce a reference value of the kinematic viscosity, ν_0, evaluated at the mean temperature and mean height of the cell. Using this reference viscosity we introduce the dimensionless viscosity ratio $\pi = \nu/\nu_0$.

When the governing equations for a vorticity-stream function formulation are put in dimensionless form two dimensionless parameters are introduced:

$$Ra = g\alpha(T_h' - T_0')\,h^3/\nu_0\kappa, \quad Pr = \nu_0/\kappa.$$

For application to mantle convection it is appropriate to consider the limit of large Prandtl number; in addition, we seek steady solutions such that $\partial/\partial t = 0$. Accordingly, the equations in the Boussinesq approximation reduce to

$$u = \partial\psi/\partial y, \quad v = -\partial\psi/\partial x, \tag{1}$$

$$w = -\nabla^2\psi, \tag{2}$$

$$\nabla^2(\pi w) = -Ra\frac{\partial T}{\partial x} - 2\left[\frac{\partial^2\pi}{\partial x^2}\frac{\partial u}{\partial y} - \frac{\partial^2\pi}{\partial y^2}\frac{\partial v}{\partial x} + \frac{\partial^2\pi}{\partial x\,\partial y}\left(\frac{\partial v}{\partial y} - \frac{\partial u}{\partial x}\right)\right], \tag{3}$$

$$\partial(uT)/\partial x + \partial(vT)/\partial y = \nabla^2 T. \tag{4}$$

Viscous dissipation and internal heat generation have been neglected in writing the energy equation (4). A numerical solution of (1) to (4) will be obtained using ψ, w and T as dependent variables. The form of the solution depends upon the prescribed viscosity function π and the parameter Ra.

A complete specification of the problem requires boundary conditions. We will take the horizontal boundaries to be free surfaces; that is, the tangential component of the shear stress vanishes. The resulting boundary conditions are $\psi = w = 0$, $T = 1$ at $y = 0$ and $\psi = w = 0$, $T = 0$ at $y = 1$. Although the fluid is of infinite horizontal extent, it is necessary to restrict our numerical solution to a finite region. We assume that the flow is periodic with a wavelength L. We further assume that each region of width L consists of two mirror image flows of width $\frac{1}{2}L$. Thus a solution will be obtained in the region $0 \leqslant y \leqslant 1$ and $0 \leqslant x \leqslant L/2h$ with the following symmetry conditions on the vertical boundaries: $\psi = w = \partial T/\partial x = 0$ at $x = 0, L/2h$. Our analysis will be restricted to the case $L/2h = 1{\cdot}4$; this corresponds approximately to one-half the wavelength for the onset of thermal convection, $L/2h = \sqrt{2}$, in a constant property fluid.

Foster (1969*b*) has examined the range of aspect ratios over which a single cell can exist for constant property thermal convection.

Several simplifying assumptions have been made; among them two-dimensionality and fixed aspect ratio. It appears that mantle convection can be approximated by two-dimensional rolls (Oxburgh & Turcotte 1968). However, the observed aspect ratio may be considerably larger than 1·4. The actual aspect ratio is determined by more general constraints such as lateral boundaries or time history. Inasmuch as rigorous guidelines for the structure of the cells are not yet available, care should be exercised in interpreting the numerical results to be presented later.

Finite difference representations of (1) to (4) were developed which led to efficient and stable computations. Central space differences were used everywhere except for the convection terms on the left side of (4). For these terms a special three point non-central difference method described by Torrance (1968) was employed. As with all differencing techniques, a truncation error appears which requires computations with a sequence of refined grids to establish quantitative validity. Assuming a given flow configuration of T, w, ψ and π throughout the mesh, the calculation proceeds by extrapolating T and w using one Gauss–Seidel and one Jacobi iteration, respectively, of difference forms of (4) and (3). For viscosity functions π with a strong dependence on T or depth, only a fraction of the Jacobi advancement of w could be used in order to preserve numerical stability. The exact fraction depended upon the particular π function being studied, and will be referred to as the fraction-of-Jacobi (F.O.J.) factor. The ψ values are then made current with T and w by using optimized successive over-relaxation to simultaneously satisfy a difference form of (2) for all points in the mesh. The velocities and viscosity π are then updated using the new fields of ψ and T. The numerical program can then proceed with a further iterative extrapolation. Numerical stability in the sense of Lax & Richtmyer (1956) follows for the various iterations provided the viscosity π does not change too much from iteration to iteration. Such stability implies convergence of the numerical results to the solution of the partial differential equations as the mesh is refined. Recognizing that large π variations may require a fine mesh in some regions and a coarse mesh in others, the numerical method was designed to transform co-ordinates from an x, y plane with a non-uniform mesh to a χ, ξ plane with a uniform mesh by using analytic transformations (usually cubic polynominals).

The numerical computations are summarized in table 1. A variety of spatial grids ranging from an 8×6 uniform array to a 22×16 non-uniform array were used. Fraction-of-Jacobi (F.O.J.) factors and the total number of iterations are also listed. The last column gives the run number of the field used as an initial guess for the iteration procedure. The first two runs were started from quiescent (no motion) fields. The first run used $T = 0$ for the initial fluid temperature and the static conduction field was computed. The second run started from the static conduction temperature field $T = 1 - y$ with a perturbation introduced at one grid point and a convection solution was computed. This constant viscosity solution was used as initial data for a number of other runs.

An important aspect of the flows is the effect of convection on the heat flux between the horizontal boundaries. This flux can be expressed in terms of a Nusselt number, Nu, defined as

$$Nu = \frac{2h}{L}\int_0^{L/2h}\left(vT - \frac{\partial T}{\partial y}\right)dx, \tag{5}$$

Run	Ra	π equation	C	Nu	Grid	Minimum F.O.J. factor	Iterations	Initial guess
1	3600	(6)	0	1·000	$15\times 11u$†	1·4	400	—
2	3600	(6)	0	3·428	$8\times 6u$	1·3	80	—
3	3600	(6)	3	2·96	$8\times 6u$	1·0	100	2
4	3600	(6)	6	2·25	$8\times 6u$	0·4	160	3
5	3600	(6)	10	2·25	$8\times 6u$	0·02	690	4
6	3500	(7)	3	2·90	$8\times 6u$	0·6	80	2
7	3500	(7)	6	1·81	$8\times 6u$	0·6	110	6
8A	3500	(7)	10	1·16	$8\times 6u$	0·2	800	7
8B	3500	(7)	10	—	$8\times 6u$	0·05	2000	2
9A	3500	(9)		1·70	$8\times 6u$	0·001	5400	4
9B	3500	(9)		1·70	$8\times 6u$	0·002	1400	2
10	3500	(9)		1·69	$15\times 11u$	0·04	600	9A
11	3500	(9)		1·72	$15\times 11n$	0·04	500	10
12	10^4	(9)		2·18	$15\times 11n$	0·04	500	11
13	$3{\cdot}5\times 10^4$	(9)		2·78	$15\times 11n$	0·03	700	12
14	10^5	(9)		3·33	$15\times 11n$	0·02	700	13
15	10^5	(9)		3·36	$22\times 16n$	0·02	400	14
16	10^6	(9)		4·58	$15\times 11n$	0·01	800	14
17	10^6	(9)		4·98	$22\times 16n$	0·01	2300	16
18	10^7	(9)		6·02	$15\times 11n$	0·01	1100	16
19	10^7	(9)		6·61	$22\times 16n$	0·01	1500	18
20	10^8	(9)		—	$15\times 11n$	0·005	3600	18

† u and n refer to uniform or non-uniform grid spacing.

TABLE 1. Summary of numerical calculations

where the integrand is the vertical heat flux at a given height y due to convection and conduction. The same finite differences were used to evaluate the integrand as were used to solve the energy equation (4). Since energy is conserved within the grid system and there is no heat flux through the vertical boundaries, the Nusselt numbers computed from (5) are invariant with y at steady state. This provided a convenient means of monitoring the approach to steady conditions. The steady values of Nu are listed in table 1.

3. Numerical results

3.1. *Temperature-dependent viscosity*

We first consider the effect of a strongly temperature-dependent viscosity. We assume the exponential form

$$\pi = \exp\left[C(\tfrac{1}{2} - T)\right]. \tag{6}$$

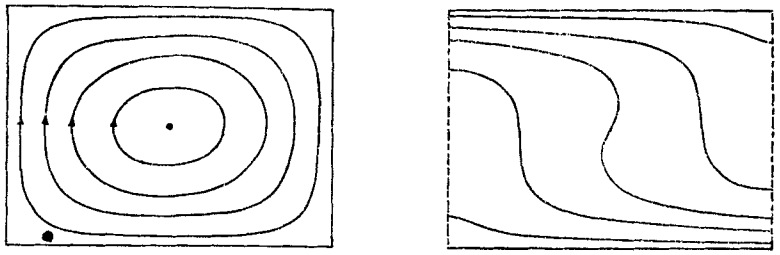

(*a*) $C=0, \psi_{\min}=-11{\cdot}2$

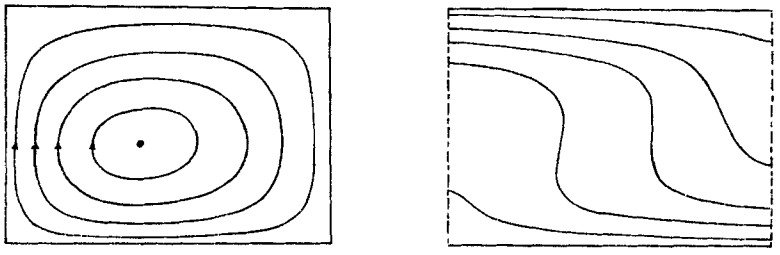

(*b*) $C=3, \psi_{\min}=-9{\cdot}8$

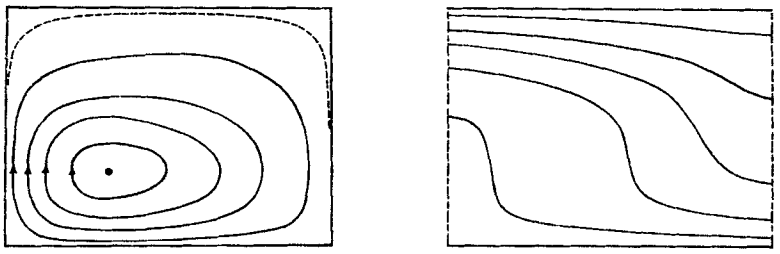

(*c*) $C=6, \psi_{\min}=-9{\cdot}7$

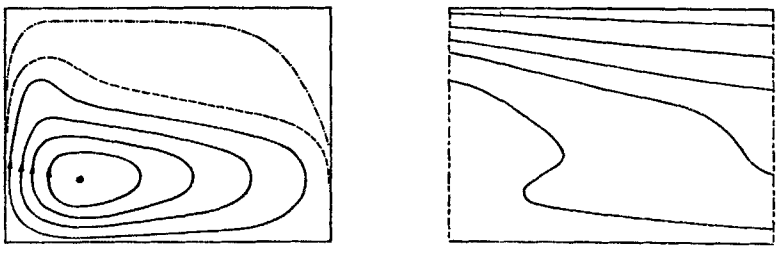

(*d*) $C=10, \psi_{\min}=-24{\cdot}5$

FIGURE 1. Streamlines and isotherms for the temperature dependent viscosity given by (6), $Ra = 3600$. Solid streamlines correspond to $\psi/\psi_{\min} = \frac{1}{8}, \frac{3}{8}, \frac{5}{8}$, and $\frac{7}{8}$; dashed and dot-dashed streamlines correspond to 0·01 and 0·001. Isotherms correspond to T = 0, 0·1, 0·3, 0·5, 0·7, 0·9 and 1.0.

The viscosity is a maximum at the upper boundary and a minimum at the lower boundary. Numerical solutions were obtained for several values of C corresponding to different ratios of maximum to minimum viscosity and for a Rayleigh number of 3600. This value was chosen because it is large compared to the critical value for constant viscosity, 657·5, yet small enough to allow the use of a fairly coarse grid in the numerical calculations.

The results of the numerical computations are shown in figure 1. The case $C = 0$ corresponds to a flow with constant viscosity and is included for comparison purposes. For $C = 3$, 6 and 10 the viscosity varies by factors of 20, 400 and 22000. In the left column of graphs streamlines are shown and in the right column isotherms. A comparison of streamlines and isotherms for $C = 0$ and $C = 3$ shows small but significant changes. The circulation, $|\psi_{\min}|$, decreases slightly as the fluid motion tends to concentrate in the region of lowest viscosity. This concentration is shown by the movement of the vortex centre, the dot, towards the lower left corner. Clearly the fluid temperature is highest near the lower boundary and in the rising thermal plume on the left, and this is the region of lowest viscosity. These trends continue for $C = 6$ and 10. However, the volume circulation is a minimum for $C = 6$ and increases considerably for $C = 10$. For $C = 10$ the fluid circulates rapidly in the lower left-hand corner of the cell where the effective Rayleigh number is large. Nearly parallel isotherms in the upper part of the cell indicate that heat transport is almost entirely by conduction. Note that Nu decreases as C is increased (table 1) and appears to be approximately constant for $C > 3$. This result coincides with the development of a nearly stagnant region at the top of the cell and this region acts as a thermal barrier to the transfer of heat between the horizontal boundaries.

The results obtained here for $C = 0$, constant viscosity, can be compared with the analytical results of Veronis (1966). Our steady-state Nusselt number of 3·428 is identical to the value 3·43 obtained by cross-plotting his results. In addition, the results for $C = 0$ generally agree with streamlines and isotherms given by Kuo (1961) and Fromm (1965). A detailed comparison is not possible inasmuch as different values of the parameters Ra and Pr were employed.

3.2. *Depth-dependent viscosity*

We next consider the effect of a strongly depth-dependent viscosity. Here we are motivated by the application to mantle convection. In the mantle the pressure increases strongly with depth due to the hydrostatic head; it is expected that this increase in pressure will lead to an increase in viscosity. Since pressure variations due to the flow are negligible, it is thus appropriate to replace the pressure dependence of viscosity by a depth dependence. We again assume the exponential form

$$\pi = \exp\left[C(\tfrac{1}{2} - y)\right]. \tag{7}$$

This viscosity is a minimum at the upper boundary and a maximum at the lower boundary. The values of C chosen are the same as in the previous section and the overall variation of the viscosity is the same. All solutions were obtained for a Rayleigh number of 3500.

The steady-state streamlines and isotherms are given in figure 2. As C increases from the constant viscosity case $C = 0$ (shown in figure 1) the flow remains almost symmetric about the vertical centreline of the cell; however, the flow tends to concentrate in the region of low viscosity as shown by the movement of

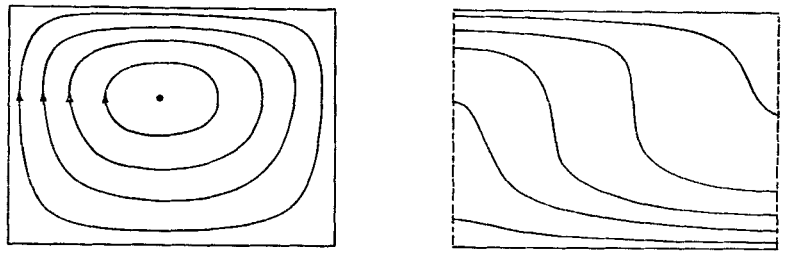

(*a*) $C=3, \psi_{\min}=-9{\cdot}1$

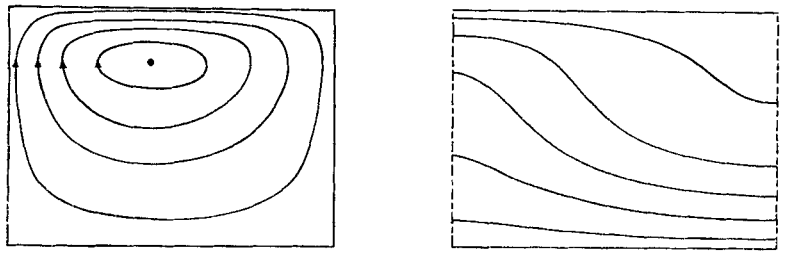

(*b*) $C=6, \psi_{\min}=-5{\cdot}5$

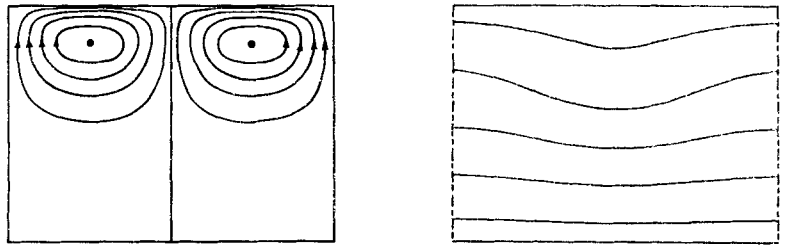

(*c*) $C=10, \psi_{\min}=-1{\cdot}9, \psi_{\max}=+1{\cdot}9$

FIGURE 2. Streamlines and isotherms for the depth dependent viscosity given by (7), $Ra = 3500$. Streamlines correspond to $\psi/\psi_{\min}$ or $\psi/\psi_{\max} = \frac{1}{8}, \frac{3}{8}, \frac{5}{8}$ and $\frac{7}{8}$. Isotherms correspond to $T = 0$, 0·1, 0·3, 0·5, 0·7, 0·9 and 1·0.

the vortex centre. The circulation decreases as C is increased. For $C = 10$ the flow splits into a pair of mirror symmetric cells. The tendency for a single convection cell to break up into multiple cells is consistent with the work of Foster (1969*a*). Foster determined the preferred horizontal wavelength for convection in a fluid with internal heating and adiabatic lower boundary. He used a viscosity expression similar to (7) and found that the preferred wavelength decreased with increasing C. The steady-state values of Nu (table 1) decrease with increasing C

as the stagnant flow region near the lower boundary becomes a more effective thermal barrier.

For $C = 10$ (run 8A), the flow developed a periodic oscillation early in the iterative transient (starting from the steady-state solution for $C = 6$) which damped out with time. To investigate the double cells and the oscillations in the flow, a second $C = 10$ run (run 8B) was carried out using the constant viscosity, $C = 0$, solution as initial data. The resulting iterative transient developed a regular periodic behaviour of large amplitude which neither grew nor decayed

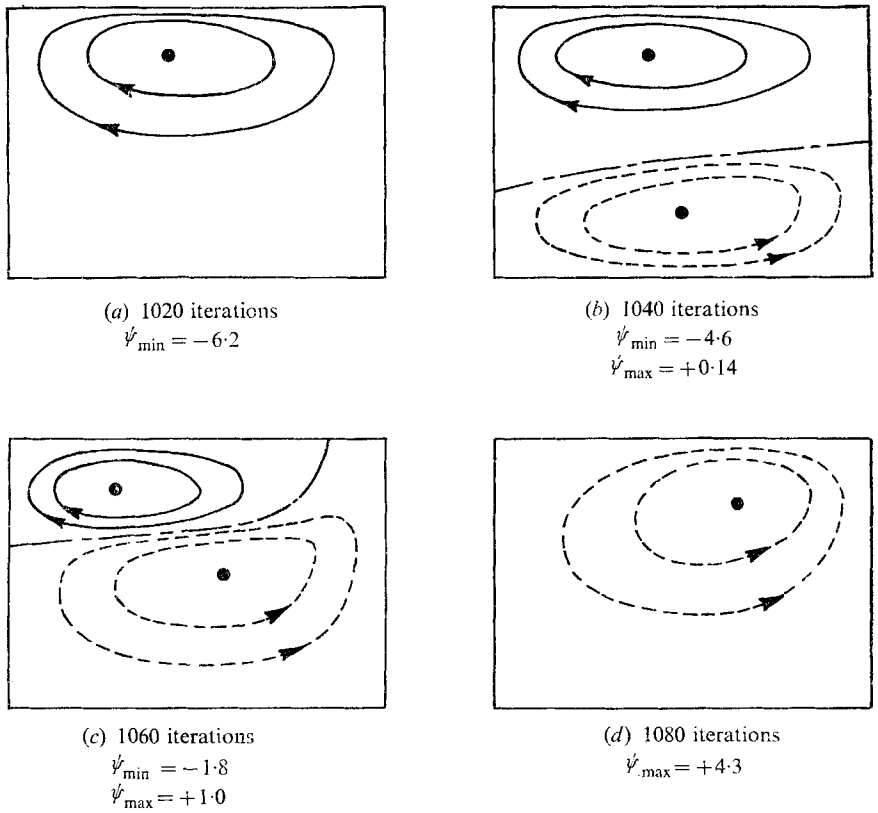

FIGURE 3. Streamlines for the period flow of run 8B. Solid streamlines correspond to $\psi/\psi_{min} = \frac{1}{3}$ and $\frac{2}{3}$; dashed streamlines correspond to $\psi/\psi_{max} = \frac{1}{3}$ and $\frac{2}{3}$.

with time. After several cycles, an artificial damping was introduced by suddenly changing the F.O.J. factor to a large value. The oscillation was interrupted and eventually decayed to the two-cell solution shown in figure 2. Justification for interpreting the iterative transient as a time-like transient is provided by the work of Garabedian (1956) and others who noted a close similarity between the development of iterative solutions of steady equations and actual time-dependent solutions. The iterative transient behaves like a real fluid transient and the number of iterations is thus a distorted 'time scale'.

The oscillation in the transient has a period between peaks of about 160

iterations. Streamlines for a half-period interval of 80 iterations are shown in figure 3; clockwise circulation is shown as solid lines, counterclockwise as dashed lines. Figure 3 clearly portrays a single cell motion in 3(*a*), the birth of a second cell in 3(*b*), its growth in 3(*c*), and its eventual displacement of the first cell in 3(*d*). Another 20 iterations and the second cell would look like the mirror image of 3(*a*) and the process would start over again.

Apparently there are two solutions to the problem for $C = 10$. One is a pair of steady, counter-rotating cells (figure 2); in the other a pair of cells periodically replace each other. Which of the two flows will result appears to be a function of the initial conditions, the non-steady flow being unstable to a sizeable perturbation, in which case it decays into the steady mode.

3.3. *Temperature- and depth-dependent viscosity*

Finally we consider a temperature- and depth-dependent viscosity which may be applicable to the earth's mantle. At high temperatures and low strain rates the process of diffusion (Herring–Nabarro) creep is expected to dominate. Diffusion creep gives a linear relation between stress and rate of strain and therefore a Newtonian viscosity. This viscosity has been derived as a function of temperature and pressure by Herring (1950). Using appropriate crystalline parameters, Turcotte & Oxburgh (1969) have expressed the diffusion creep viscosity for the mantle as

$$\eta = 2{\cdot}76 \times 10^3 T' \exp\left(\frac{5{\cdot}222 \times 10^4 + 1{\cdot}087 \times 10^{-7} p}{T'}\right), \tag{8}$$

with T' in °K, p in dyne/cm^2, and η in poise.

For the numerical calculations we consider a layer 700 km thick and replace the pressure p by the hydrostatic pressure. The pressures at the top and the bottom are taken to be zero and $2{\cdot}30 \times 10^{11}$ dynes/cm^2, respectively. The temperatures at the top and bottom are taken to be 1420 and 2100 °K. These assumptions, although reasonable, neglect the presence of the cold crustal layer which has essentially infinite viscosity and a thickness of approximately 20 km. We also take the temperature in front of the exponential in (8) to be a constant equal to the mean of the boundary temperatures. This is a good approximation since the exponential temperature dependence dominates. With the above choice of temperatures on the horizontal boundaries the viscosity on the two boundaries and the reference viscosity are the same; from (8) this reference viscosity is $\eta_0 = 4{\cdot}55 \times 10^{22}$ poise. Taking the values given above, the dimensionless viscosity ratio is given by

$$\pi = 10^{-16} \exp\left(\frac{77{\cdot}4 - 25{\cdot}2y}{1{\cdot}42 + 0{\cdot}68T}\right). \tag{9}$$

From the temperature boundary conditions we have $\pi = 1$ on the horizontal boundaries. If T is a linear function of y, i.e. pure conduction, then $\pi = 1$ throughout the layer.

Computations using this model have been performed over a range of Rayleigh numbers using a variety of uniform and non-uniform grids as indicated in table 1. Results are shown in figure 4 for Rayleigh numbers of 3500, 10^4, 10^5, 10^6 and 10^7.

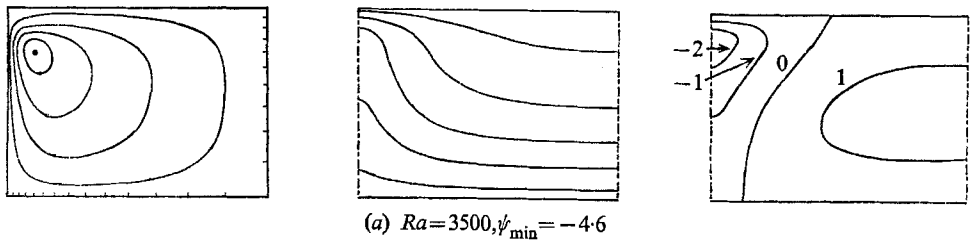

(a) $Ra=3500, \psi_{\min}=-4{\cdot}6$

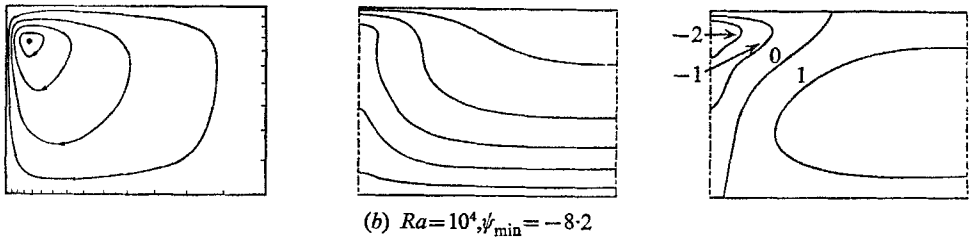

(b) $Ra=10^4, \psi_{\min}=-8{\cdot}2$

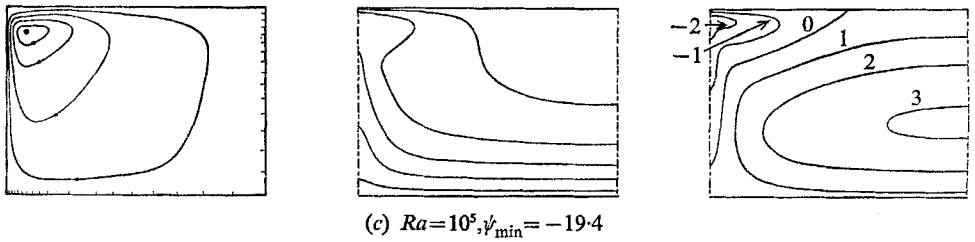

(c) $Ra=10^5, \psi_{\min}=-19{\cdot}4$

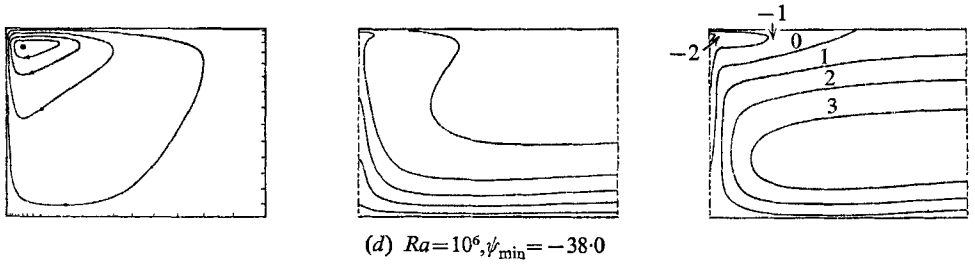

(d) $Ra=10^6, \psi_{\min}=-38{\cdot}0$

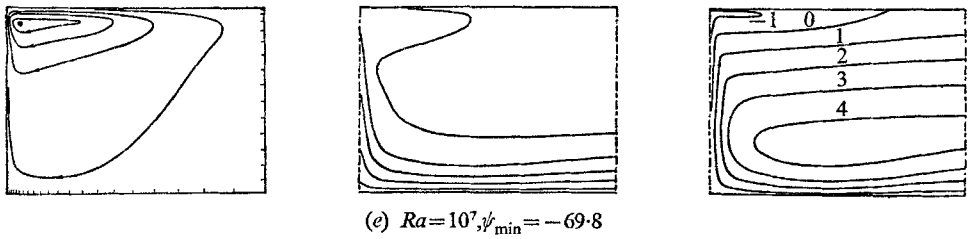

(e) $Ra=10^7, \psi_{\min}=-69{\cdot}8$

FIGURE 4. Streamlines, isotherms, and lines of constant viscosity for the temperature- and depth-dependent viscosity model (9) at various Rayleigh numbers. Streamlines correspond to $\psi/\psi_{\min} = \frac{1}{8}, \frac{3}{8}, \frac{5}{8}$ and $\frac{7}{8}$; isotherms correspond to $T = 0, 0{\cdot}1, 0{\cdot}3, 0{\cdot}5, 0{\cdot}7, 0{\cdot}9$ and 10. Numbers on the constant viscosity curves denote $\log_{10}\pi$.

Certain reservations about the flow at $Ra = 10^7$ exist, these will be elaborated later. In addition to the streamlines and isotherms, the right-hand column in figure 4 gives the lines of constant viscosity in each flow. The grid used for each calculation is shown by ticks on the boundaries of the flow field.

There is relatively little change of the streamlines as the Rayleigh number is increased. The change in the magnitude of the circulation is somewhat greater. The changes with Rayleigh number of the isotherms and lines of constant viscosity are more evident. For Ra between 10^5 and 10^7 the region of low viscosity is small and confined, whereas an extended region of cold fluid appears in the upper right-hand corner and a large region near the right side is nearly stagnant. The minimum viscosity is about two orders of magnitude smaller than the reference viscosity while the maximum viscosity in the stagnant region is nearly three to four orders of magnitude larger.

The flow field for $Ra = 3500$ was obtained by sequentially refining the spatial grid (runs 9A, 10 and 11 in table 1). For run 9A the flow broke up into as many as four cells during the transient. Eventually, only one cell persisted, giving essentially the flow shown in figure 4. This remarkable transient attests to the stability of the numerical method. The computation was repeated in run 9B using a different initial field and required somewhat fewer iterations to achieve the same steady state. Obviously, the initial field of run 9B was a better guess. Once an approximate field was obtained, the grid was refined and the calculation continued. Fortunately, only a few hundred iterations were then required. If the refined grid of run 11 had been used to start from the initial data of run 9A or 9B the computer time involved would have been prohibitive. The sequence of calculations using successively refined grids appears to be an optimum. [The sequence of runs 9A, 10 and 11 required about 20 min on an IBM 360/65 computer. The calculation of the flows in §§ 3.1 and 3.2 required less than 4 min.] Note the small difference in the steady state Nu for the various grids used at $Ra = 3500$. This lends support to the validity of the results given previously using the coarse grid.

For $Ra = 10^8$ the flow began to develop a periodic oscillation of the type discussed in § 3.2. Rather than a single large eddy being generated, small eddies were periodically generated near the lower right-hand corner of the cell. The grid was not adequate to resolve the flow and the computation was terminated. Further grid refinement in run 19 at $Ra = 10^7$ revealed that the transient Nu was starting to oscillate weakly. No secondary eddies formed during the computation, but the isotherms near the lower right corner of the cell were slowly oscillating up and down in response to the fluid's efforts to develop an eddy in that region. It would appear that for $Ra \gtrsim 10^7$ multiple cells will develop.

4. Comparison with mantle convection

The numerical results presented in § 3.3 only approximate convection in the mantle. To obtain more realistic results would require relaxing some of the assumptions in the model. Nevertheless, it is possible to compare some aspects of the variable viscosity flows with measurements on mantle convection. The

surface heat flux and movement on the upper boundary fall in this category. Figure 5 presents the maximum horizontal velocity and maximum heat flux [in terms of a local Nusselt number $Nu_x = hq_x/k(T'_h - T'_0)$] on the upper boundary as a function of Ra. The best fits through these points are of the form $u \sim Ra^{0.63}$ and $Nu_x \sim Ra^{0.31}$, respectively.

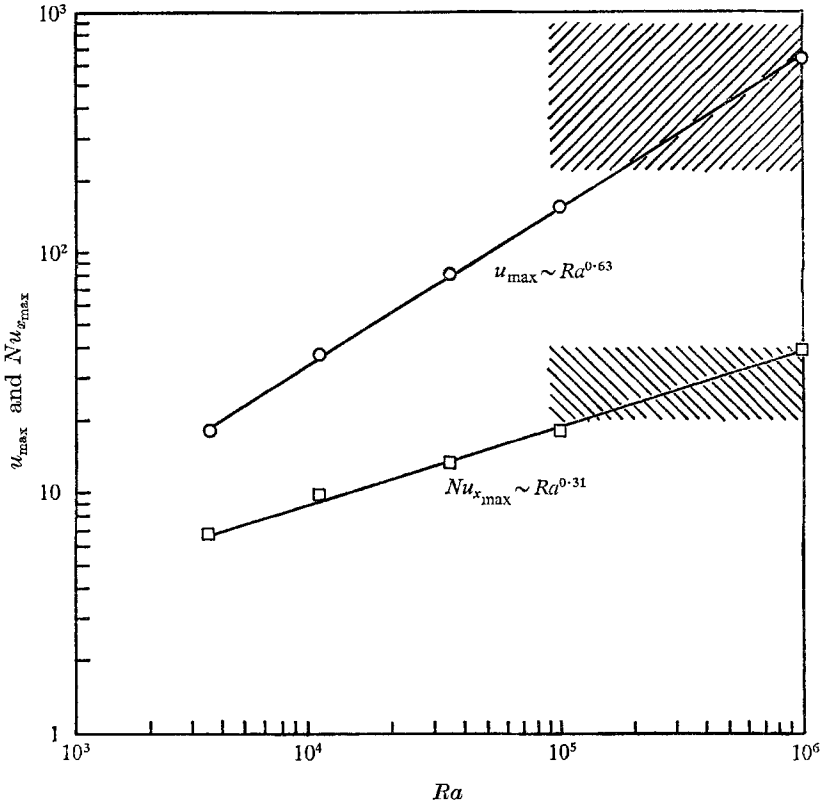

FIGURE 5. Maximum calculated values of local Nusselt number, Nu_x, and horizontal velocity, u, along the upper boundary of the cell versus Rayleigh number for the mantle viscosity model (9). Cross-hatched bands indicate the range of measurements of maximum heat flux to the ocean floor and range of observed spreading velocities of the ocean floor away from ridges.

Typical velocities of ocean floor movement away from ocean ridges are 1–4 cm/yr (Vine 1966) and maximum values of the surface heat flux (which occur at the ridges) are 2–4 μcal/cm^2 sec (Lee & Uyeda 1965, Von Herzen & Langseth 1965). Using $h = 700$ km, $\kappa = 10^{-2}$ cm^2/sec, $T'_h - T'_0 = 680$ °K, and $k = 10^{-2}$ cal/cm sec °K, the observed values are put in dimensionless form and are shown as cross-hatched bands in figure 5. Observed values of both quantities correspond to a range of Rayleigh numbers between 10^5 and 10^6, thus lending some support to the validity of the numerical results.

The authors would like to acknowledge Cornell University for providing necessary computer time. This work was also supported in part by National Science Foundation Grant GK 4656 and by AFOSR F44620-69-C-0063.

REFERENCES

ELDER, J. W. 1968 *Sci. Prog.* **56**, 1.

FOSTER, T. D. 1969*a* *J. Geophys. Res.* **74**, 685.

FOSTER, T. D. 1969*b* *J. Fluid Mech.* **37**, 81.

FROMM, J. E. 1965 *Phys. Fluids*, **8**, 1757.

GARABEDIAN, P. R. 1956 *Math. Tables Aids Comp.* **10**, 183.

GORDON, R. B. 1965 *J. Geophys. Res.* **70**, 2413.

HERRING, C. 1950 *J. Appl. Phys.* **21**, 437.

ISACKS, B., OLIVER, J. & SYKES, L. R. 1968 *J. Geophys. Res.* **73**, 5855.

KUO, H. L. 1961 *J. Fluid Mech.* **10**, 611.

LAX, P. D. & RICHTMYER, R. D. 1956 *Commun. Pure Appl. Math.* **9**, 267.

LE PICHON, X. 1968 *J. Geophys. Res.* **73**, 3661.

LEE, W. H. K. & UYEDA, S. 1965 In *Terrestrial Heat Flow*, pp. 58–77. American Geophysical Union, Washington.

LIANG, S. F., VIDAL, A. & ACRIVOS, A. 1969 *J. Fluid Mech.* **36**, 239.

MCKENZIE, D. P. 1969 *Geophys. J. Roy. Astr. Soc.* **18**, 1.

MCKENZIE, D. P. & PARKER, R. L. 1967 *Nature, Lond.* **216**, 1276.

MORGAN, W. J. 1968 *J. Geophys. Res.* **73**, 1959.

OXBURGH, E. R. & TURCOTTE, D. L. 1968 *J. Geophys. Res.* **73**, 2643.

TORRANCE, K. E. 1968 *J. Res. Nat. Bur. Stand.* **72B**, 281.

TURCOTTE, D. L. & OXBURGH, E. R. 1969 *J. Geophys. Res.* **74**, 1458.

VERONIS, G. 1966 *J. Fluid Mech.* **26**, 49.

VINE, F. J. 1966 *Science, N.Y.* **154**, 1405.

VON HERZEN, R. P. & LANGSETH, M. G. 1965 *Phys. Chem. Earth*, **6**, 365.